Supporting Information

Polypyrrole-Encapsulated Amorphous Bi_2S_3 Hollow Sphere for Long Life Sodium Ion Battery and Lithium-Sulfur Battery

Bei Long,[a] Zhengping Qiao,[a] Jingnan Zhang,[a] Shanqing Zhang,[c] Muhammad-Sadeeq Balogun,[d] Jun Lu,*[b] Shuqin Song*[a] and Yexiang Tong*[a]

[a]The Key Lab of Low-Carbon Chemistry & Energy Conservation of Guangdong Province, MOE of the Key Laboratory of Bioinorganic and Synthetic Chemistry, KLGHEI of Environment and Energy Chemistry, School of Materials Science and Engineering, School of Chemistry, Sun Yat-sen University, Guangzhou 510275 P. R. China. E-mail: S.Q. Song: stsssq@mail.sysu.edu.cn; Y.X. Tong: chedhx@mail.sysu.edu.cn

[b]Chemical Sciences and Engineering Division, Argonne National Laboratory, Argonne, Illinois 60439, USA. E-mail: junlu@anl.gov

[c]Centre for Clean Environmental and Energy and School of Environment and Science, Griffith University, Gold Coast, Queensland, 4222, Australia

[d]College of Materials Science and Engineering, Hunan University, Changsha 410012 P. R. China

The formation mechanism of BiG sphere.

During the hydrothermal process, Bi-PVP complexes were generated by the coordinative bonding with the carbonyl oxygen of PVP.[1] The superfluous PVP coated the Bi-PVP complexes to generate micelles in the solvent. Meanwhile, Bi^{3+} also combined with glycol by complexation reaction.[2] Then, the crystal gradually grew up and finally generated BiG sphere.

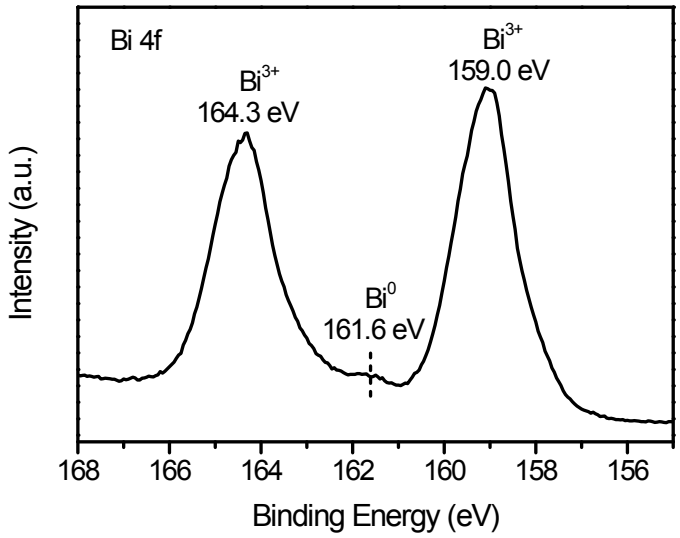

Fig. S1 Bi 4f XPS spectrum of BiG sphere.

The Bi 4f XPS spectrum of BiG sphere is shown in Fig. S1, the strong characteristic peaks at 164.3 and 159.0 eV are attributed to Bi^{3+}, while the weak peak at 161.6 eV belongs to metal Bi^{0}.[3] The glycol with reducibility leads to the generation of metal Bi^{0}. Thus, elemental Bi in BiG sphere exists in the form of major Bi^{3+} and a handful of Bi^{0}.

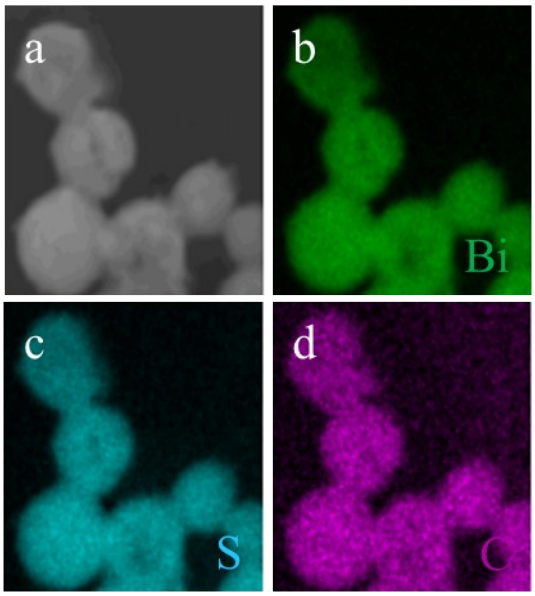

Fig. S2 Elemental mappings of Bi_2S_3 HS.

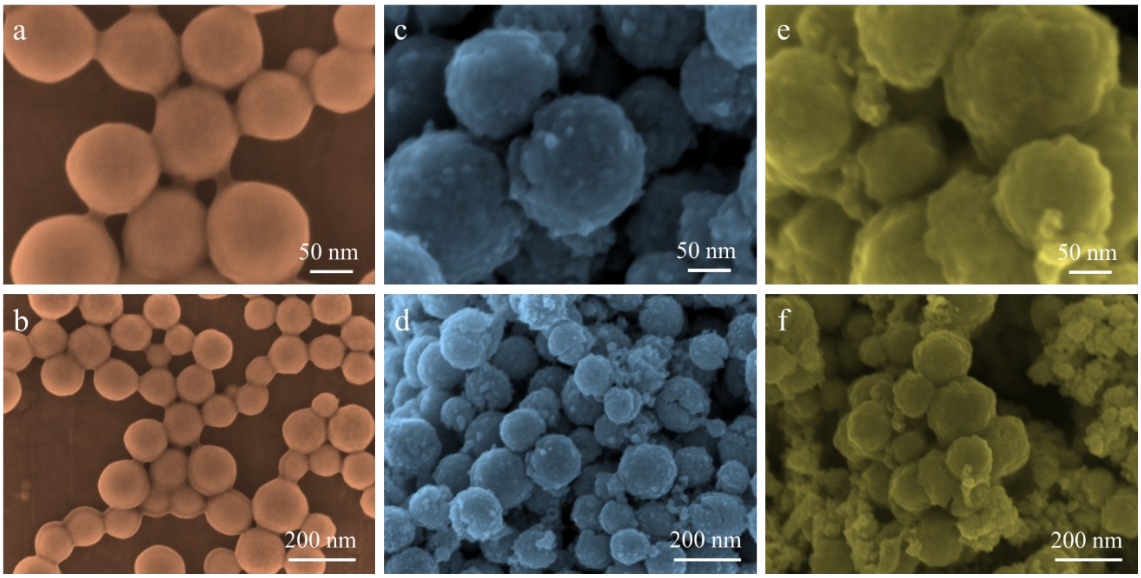

Fig. S3 SEM images of (a,b) BiG sphere, (c,d) Bi_2S_3 HS and (e,f) Bi_2S_3-PPy HS.

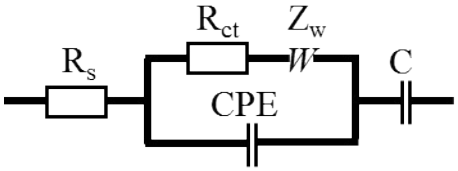

Fig. S4 Modeled equivalent circuit of EIS.

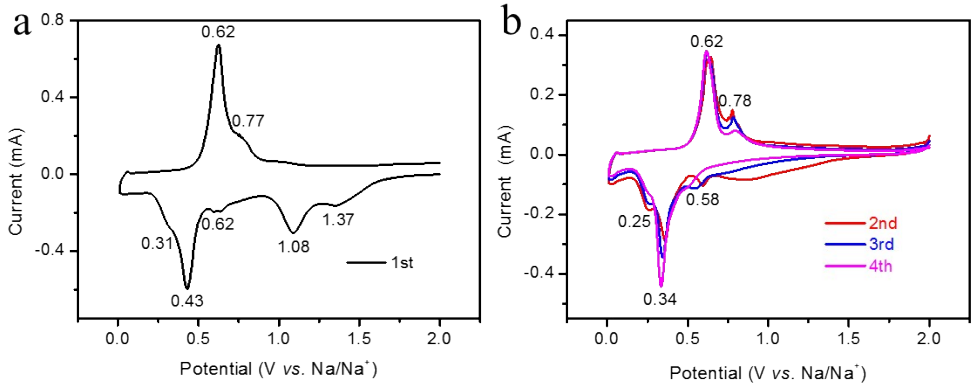

Fig. S5 CV curves of Bi_2S_3 HS.

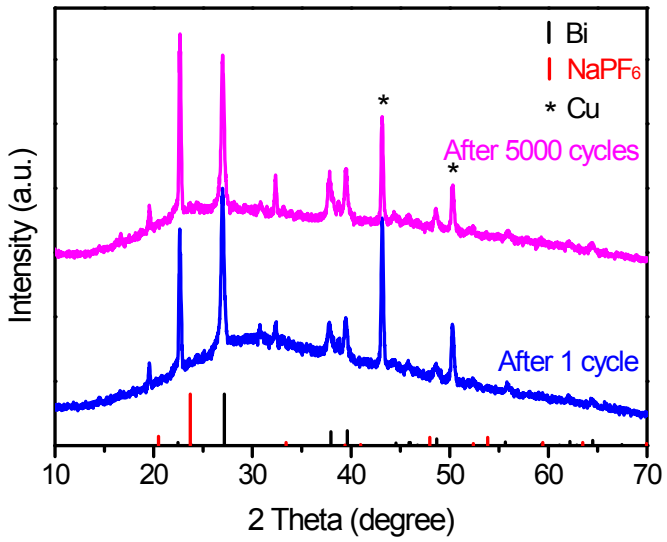

Fig. S6 XRD spectra of Bi_2S_3-PPy HS after cycling.

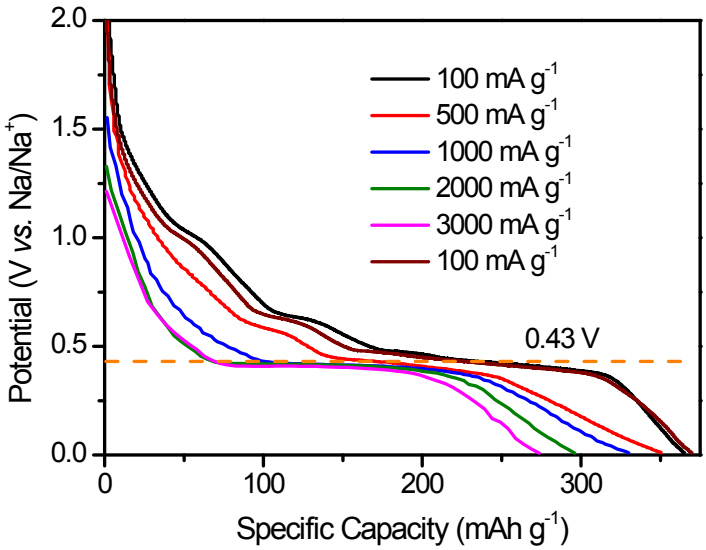

Fig. S7 Discharging curves at different current densities of Bi_2S_3-PPy HS.

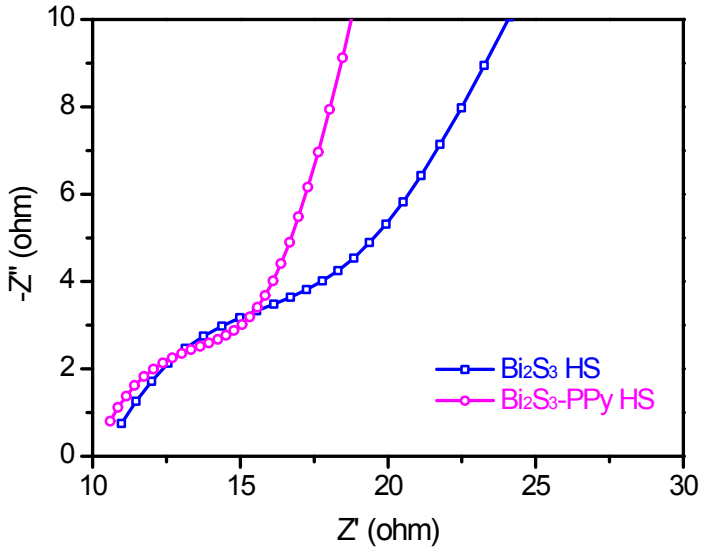

Fig. S8 EIS spectra of Bi_2S_3 HS and Bi_2S_3-PPy HS.

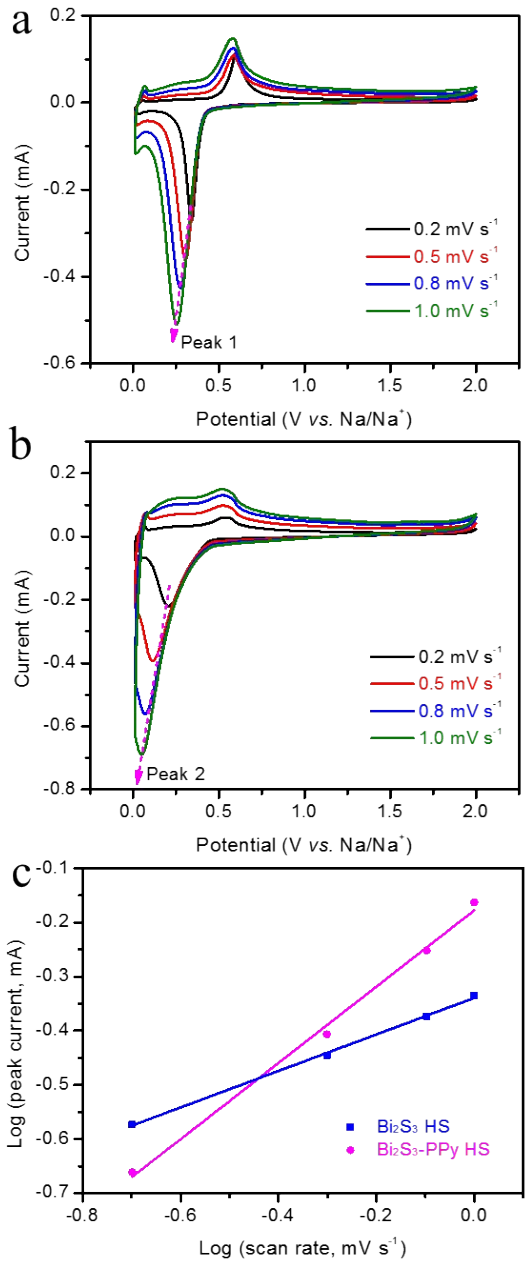

Fig. S9 CV curves of (a) Bi_2S_3 HS and (b) Bi_2S_3-PPy HS at different scan rates. (c) Log plot of peak 1 and peak 2 currents versus scan rates.

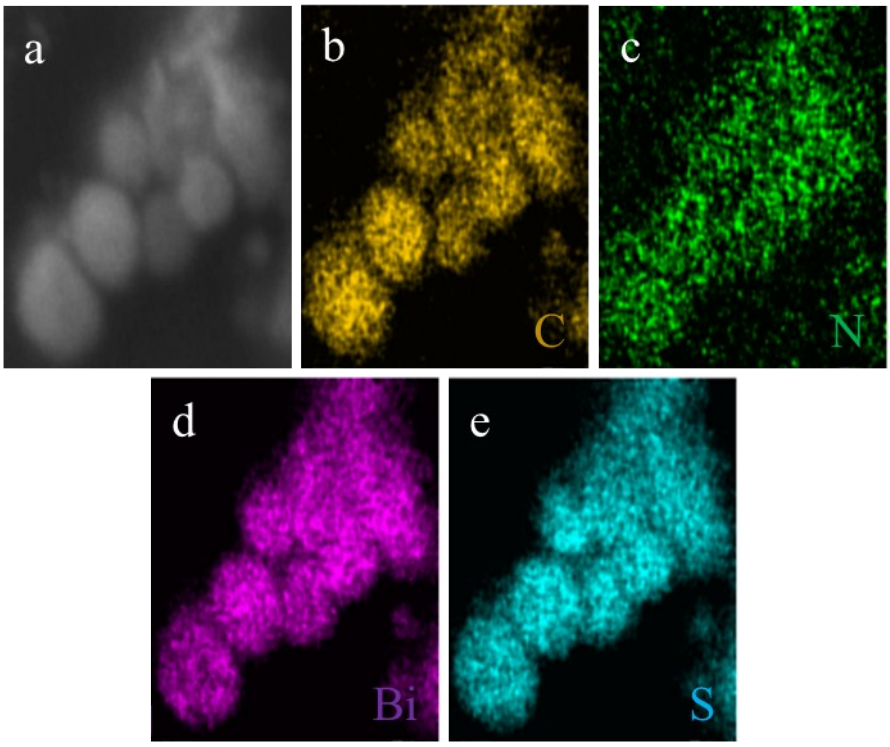

Fig. S10 Elemental mappings of Bi_2S_3-PPy HS/S.

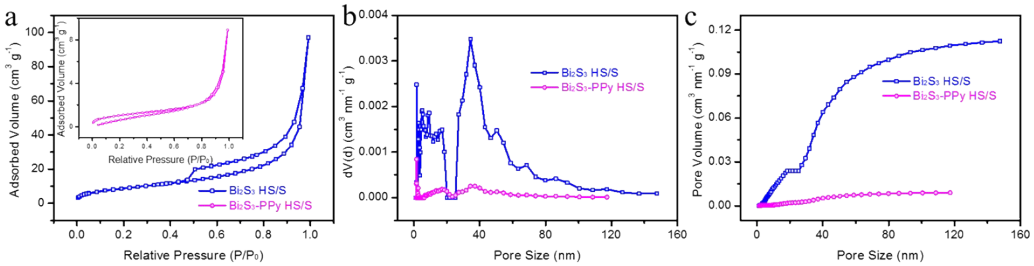

Fig. S11 (a) N_2 adsorption-desorption isotherms, pore size distribution and cumulative pore volume plots of Bi_2S_3-PPy HS and Bi_2S_3-PPy HS/S.

As shown in Fig. S11a, the N_2 adsorption-desorption isotherms reflect a polyporous structure of Bi_2S_3-PPy HS compared to Bi_2S_3-PPy HS/S. The specific surface areas of Bi_2S_3-PPy HS and Bi_2S_3-PPy HS/S are 0.6864 and 0.0638 m^2 g^{-1}. The Fig. S11b indicates that Bi_2S_3-PPy HS has a number of differently-sized pores. The micropores and mesopores are derived from the porous surface of Bi_2S_3 and PPy. The macropores

are attributed to the hollow structure of Bi_2S_3. Meanwhile, Bi_2S_3-PPy HS has an obviously bigger pore volume than that of Bi_2S_3-PPy HS/S (Fig. S11c). These reveal that the most pores have been occupied by sulfur after the sulfur infiltration.

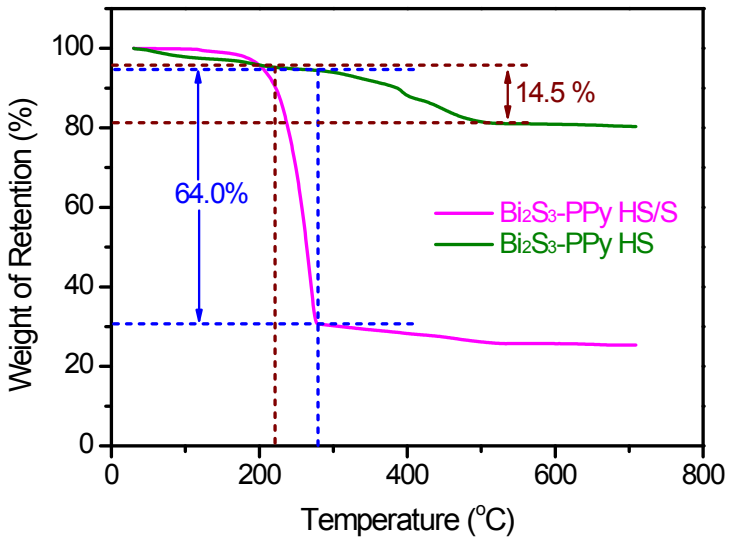

Fig. S12 TGA curves of Bi_2S_3-PPy HS and Bi_2S_3-PPy HS/S.

The thermogravimetric analysis (TGA) curves of Bi_2S_3-PPy HS and Bi_2S_3-PPy HS/S are collected to present the fractions of Bi_2S_3, PPy and S in the Bi_2S_3-PPy HS/S, as displayed in Fig. S12. The decomposition temperature of PPy is about 220 °C.[4] Thus, the content of PPy in Bi_2S_3-PPy HS is about 14.5%. The weight loss before 220 °C is ascribed to the water evaporation (4.1%). While the complete vaporization of S in Bi_2S_3-PPy HS/S is finished at 281 °C. The weight loss of Bi_2S_3-PPy HS/S from the room temperature to 281 °C contains the S sublimation, the water evaporation and the decomposition of PPy. By subtracting the weight change of Bi_2S_3-PPy HS in this temperature range, we get the content of S (64.0%) in Bi_2S_3-PPy HS/S. As a result, the fractions of H_2O, Bi_2S_3, PPy and S in the Bi_2S_3-PPy HS/S composite are about 1.4%, 29.4%, 5.2% and 64.0%.

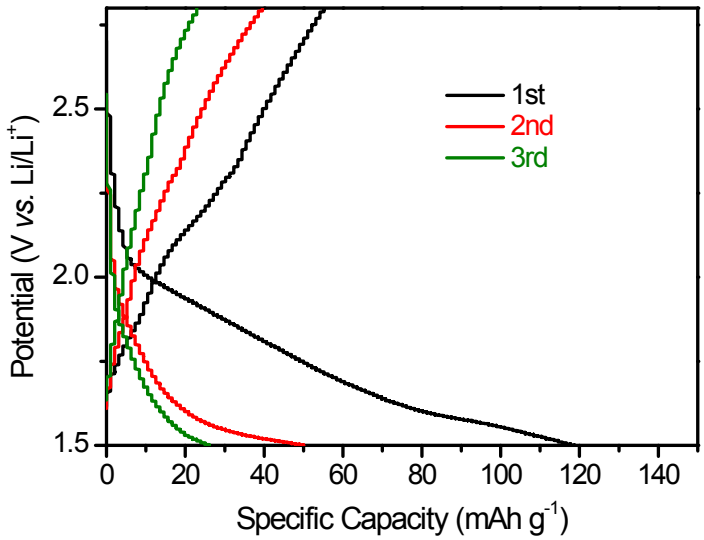

Fig. S13 Charging-discharging curves of Bi_2S_3 HS in Li-S battery.

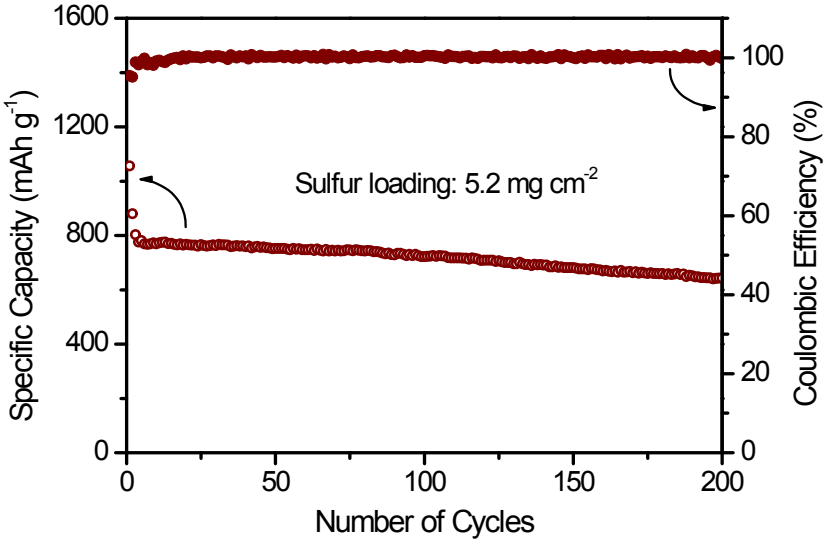

Fig. S14 Cyclic life of Bi_2S_3-PPy HS/S with mass loading of 5.2 mg cm^{-2} at 1 C.

Table S1 A comparison of cycling performance of Bi-based anode in sodium ion batteries

Electrode	Current Density (mA g^{-1})	Number of Cycles	Final Capacity (mAh g^{-1})	Capacity Retention	Reference
Bi_2S_3-PPy hollow sphere	1000	5000	306	90%	This work
Bi_2S_3-PPy yolk-shell composites	313	100	380	61%	[5]
Bi_2S_3/C	120	100	379	45%	[6]
$Bi_{0.94}Sb_{1.06}S_3$/ C	1000	200	410	60%	[7]
Bi_2S_3	100	40	322	52%	[8]
np-Bi_2Sb_6	1000	10000	150	28%	[9]
Bulk Bi	400	2000	389	94%	[10]
Bi@C microsphere	100	100	123.5	48%	[11]
Bi-NS@C composite	200	1000	106	20%	[12]
Bi@Graphite	3200	10000	144	90%	[13]
arrayed Bi nanorod	50	150	302	83%	[14]
Bi/C nanofibers	100	500	273	46%	[15]
Bi/CNFs	50	100	186	50%	[16]

References

1. F. Qin, G. Li, H. Xiao, Z. Lu, H. Sun and R. Chen, *Dalton Trans.*, 2012, **41**, 11263.
2. X. Jiang, Y. Wang, T. Herricks and Y. Xia, *J. Mater. Chem.*, 2004, **14**, 695.
3. F. Dong, Q. Li, Y. Sun and W.-K. Ho, *ACS Catal.*, 2014, **4**, 4341.
4. Y. Fu and A. Manthiram, *RSC Adv.*, 2012, **2**, 5927.
5. H. Liang, J. Ni, L. Li, *Nano Energy*, 2017, **33**, 213.

6. Y. Zhao, A. Manthiram, *Chem. Mater.*, 2015, **27**, 6139.

7. W. Sun, X. Rui, D. Zhang, Y. Jiang, Z. Sun, H. Liu, S. Dou, *J. Power Sources*, 2016, **309**, 135.

8. W. Li, C. Han, S. Chou, J. Wang, Z. Li, Y. Kang, H. Liu, S. Dou, *Chem. Eur. J.*, 2016, **22**, 590.

9. H. Gao, J. Niu, C. Zhang, Z. Peng, Z. Zhang, *ACS Nano*, 2018, **12**, 3568.

10. C. Wang, L. Wang, F. Li, F. Cheng, J. Chen, *Adv. Mater.*, 2017, **29**, 1702212.

11. F. Yang, F. Yu, Z. Zhang, K. Zhang, Y. Lai, and J. Li, *Chem. Eur. J.*, 2016, **22**, 2333.

12. J. Qiu, S. Li, X. Su, Y. Wang, L. Xu, S. Yuan, H. Li, S. Zhang, *Chem. Eng. J.*, 2017, **320**, 300.

13. J. Chen, X. Fan, X. Ji, T. Gao, S. Hou, X. Zhou, L. Wang, F. Wang, C. Yang, L. Chen, C. Wang, *Energy Environ. Sci.*, 2018, **11**, 1218.

14. S. Liu, J. Feng, X. Bian, J. Liu and H. Xu, *J. Mater. Chem. A*, 2016, **4**, 10098.

15. H. Yin, Q. Li, M. Cao, W. Zhang, H. Zhao, C. Li, K. Huo, and M. Zhu, *Nano Research*, 2017, **10**, 2156.

16. Y. Jin, H. Yuan, J. Lan, Y. Yu, Y. Lin and X. Yang, *Nanoscale*, 2017, **9**, 13298.